

Article

Spectrometer-Based Line-of-Sight Temperature Measurements during Alkali-Pulverized Coal Combustion in a Power Station Boiler

Weijie Yan ¹, Yunqi Ya ¹, Feng Du ², Hao Shao ³ and Peitao Zhao ^{1,*}

¹ School of Electrical and Power Engineering, China University of Mining and Technology, No. 1, Daxue Road, Xuzhou 221116, China; yanweijie@cumt.edu.cn (W.Y.); yayunqi@cumt.edu.cn (Y.Y.)

² Huadian Power International Corporation Limited Zouxian power plant, Tangcun town, Zhoucheng 273500, China; 13355113598@163.com

³ School of Safety Engineering, China University of Mining and Technology, No. 1, Daxue Road, Xuzhou 221116, China; sh0915@163.com

* Correspondence: p.zhao@cumt.edu.cn; Tel.: +86-0516-8359-2000

Academic Editor: Vasily Novozhilov

Received: 25 August 2017; Accepted: 7 September 2017; Published: 10 September 2017

Abstract: A portable spectrometer system that simultaneously measures the temperature, emissivity, and radiation intensity of an alkali metal was used in a 1000 MW coal-fired power plant boiler furnace. A calibrated fiber-optic spectrometer system was applied to obtain the radiation intensity of the flame. A simple method based on polynomial fitting was used to separate the continuous baseline from the measured flame spectra that contained both continuous and discontinuous bands. Nine synthetic spectra that included the baseline, noise, and three simulated discontinuous bands based on a Gaussian function were created to test the accuracy of the separation method. The accuracy of the estimated continuous baseline was evaluated by the goodness-of-fit coefficient quality metric. The results indicated good spectral matching for the selected profiles. The soot emissivity model by Hottel and Broughton was employed to calculate temperature and emissivity. The influence of discontinuous emission spectra on the temperature and emissivity calculations was evaluated. The results showed that the maximum difference of the measurement points of the calculated temperature was only 6 K and that the relative difference in emissivity among the measurement points was less than 5%. In addition, a comparison between the actual intensity of the alkali metal and the calculated temperature indicated that the change in the radiation intensity of the alkali metal followed the trend of the calculated temperature. This study serves as a preliminary investigation for measuring gas-phase alkali metal concentrations in a furnace.

Keywords: temperature measurement; flame spectrum; emissivity; alkali metal emission

1. Introduction

The effective detection and diagnosis of coal-fired power plant furnace flames is required for the safe operation of power plant boilers. Various methods for flame detection and diagnosis have been reported [1–5]. The laser spectroscopy method [6] has high temporal and spatial resolution, and can be used to measure temperature and to determine the concentrations of many components during the combustion process. However, expensive equipment and complex optical systems are required; therefore, this approach is not easily applied to industrial furnaces. Image processing techniques, based on a tri-chromatic signal of the image and using the two-color method, have been widely used for temperature measurements of furnace flames [7–10]. The emission from emitters at two wavelengths is utilized to calculate the temperature and emissivity in image processing techniques. However, the

radiation energy of the tri-chromatic signal is not exactly monochromatic and the wavelengths of the tri-chromatic signal may vary between different image acquisition systems [11]. Additionally, the method fails to detect radical radiation in the flame. A fiber-optic spectrometer system with a simple structure, low data processing requirements, and an ability for gathering additional information may be more useful for flame diagnosis. At the same time, this method can achieve an online detection of temperature and emissivity, as well as radical radiation for certain components, such as CH^* , C_2^* , Na^* , and K^* .

Flame spectra are classified depending on the energy distribution of continuous and discontinuous spectra [12]. For continuous spectra, the emitted or absorbed energy is distributed in a continuous spectrum over a wide wavelength region. The emitted or absorbed energy is mainly concentrated in a narrow band of the spectrum in discontinuous spectra [13]. Usually, a continuous spectrum represents low-frequency components and the discontinuous emission is characterized by high-frequency components [14]. The continuous spectrum of a coal-fired flame that is usually applied to calculate temperature provides important information for soot formation [15]. The existence of discontinuous emission spectra may influence the temperature calculation's accuracy. On the other hand, supercritical power station boilers are very prone to the coking phenomenon due to very high temperatures and a low ash fusion point in the fuel. The ash fusion point is closely related to the alkali metal content of the fuel. Oleschko et al. [16] found that alkali metals released during combustion are responsible for the formation of sticky deposits in the boiler. Therefore, accurate measurements of the concentrations of the alkali metal, such as Na^* and K^* , in a flame are very important for the prevention of deposits that interfere with the proper function of the furnace. The radiation intensity of alkali metals in the furnace flame is not only related to the concentration of the alkali metal vapor but also to the local flame temperature. Building a functional expression between these three parameters can achieve online measurements of the concentration of the alkali metal. However, the continuous and discontinuous spectra are superimposed, but the flame temperature and the actual radiation intensity of the alkali metals depend on continuous and discontinuous spectra. Thus, it is necessary to separate the continuous and discontinuous spectral information from the measured flame spectrum. There are automated and manual methods for separating the discontinuous and continuous spectra in the spectra of coal-fired flames [17]. Automated methods can automatically estimate a continuous baseline from the measured flame spectra, while manual approaches require operator intervention for the selection of several baseline points. Both methods are highly sensitive to signal parameters such as noise [13].

An emissivity model is required to calculate temperature and emissivity based on a continuous spectrum. Two popular emissivity models have been applied to coal-fired flames. Most researchers have assumed a coal flame to be a gray body emitter with a constant emissivity [18–20]. Hottel and Broughton's soot emissivity model [21], which is spectrally dependent, is another popular model for radiating soot particles. Nevertheless, no single existing emissivity model can be used in every situation. In fact, the effective implementation of spectrum technology to measure the temperature in a coal flame is dependent on the kinds of emitters present. Generally, visible radiation from coal flames derived from particles such as coal, char, ash, and soot are generated during coal combustion [22]. Backstrom et al. [23] reported that the particle radiation within a flame depended not only on the particle concentration and particle temperature, but also on the type of particles, or more precisely, their radiative properties.

Soot particles with strong absorption and emission characteristics and in relatively small quantities are assumed to dominate the emissions. Soot in a coal flame typically consists of individual particles or agglomerates comprised of between several and thousands of primary particles [24]. The diameter of individual soot particles is about 20–40 nm, and coal, char, and ash particles are about 2–500 μm [25]. Therefore, soot particles are significantly smaller than the accompanying coal and char particles and can be optically isolated [4]. However, the soot cloud generated by the decomposition of volatile substances in a high-temperature environment produces a semi-transparent media with an associated

equivalent. At the same time, the small size of soot particles produces a larger total surface area and enhances the radiative heat transfer. Fletcher [24] concluded that, in the presence of a large radiant surface area, the near-burner flame temperature could be lowered several hundred degrees due to the heat transfer to the surrounding walls. Draper [22] reported that two models for coal combustion flame were not ideal, but that Hottel and Broughton's soot emissivity model was more suitable and accurate than Gray's model for the image processing of flame images near the burner.

A simple manual method for spectral separation is proposed and validated in this study. Hottel and Broughton's emissivity model is applied to obtain the temperature and emissivity of a furnace flame based on estimated continuous spectra. The influence of the discontinuous emission spectra on the calculation of flame temperature and emissivity is also discussed. Finally, the relationship between the temperature and intensity of an alkali metal is discussed.

2. Measurement Principle

The emissive power distribution of a blackbody for a given wavelength can be represented using Planck's law [22]:

$$E_{\lambda,b}(T, \lambda) = \frac{C_1 \lambda^{-5}}{\exp \frac{C_2}{\lambda T} - 1} \quad (1)$$

where $E_{\lambda,b}(T, \lambda)$ is the spectral emissive power of a blackbody (W/m^{-3}), λ is the wavelength (m), T is temperature (K), and $C_1 = 3.7419 \times 10^{-16} \text{W} \cdot \text{m}^2$ and $C_2 = 1.4388 \times 10^{-2} \text{m} \cdot \text{K}$ are called Planck's first and second radiation constant, respectively. However, particles in a pulverized coal flame do not emit blackbody radiation, and the actual spectral emissive power of a non-blackbody is the emissive power of a blackbody multiplied by the spectral emissivity ε_λ that can be expressed as follows:

$$E_\lambda(T, \lambda) = \varepsilon_\lambda E_{\lambda,b}(T, \lambda). \quad (2)$$

The emissive power is inadequate to describe the directional dependence of the radiation field, especially inside an absorbing/emitting medium, where photons may not have originated from a surface [26]. Therefore, a related concept that is very similar to the emissive power is the radiative intensity. The relationship between the intensity of a non-blackbody and its emissive power can be expressed as follows [26]:

$$I_\lambda(T, \lambda) = \frac{1}{\pi} E_\lambda(T, \lambda). \quad (3)$$

In a widely used method, Hottel and Broughton developed an empirical emissivity model shown in Equation (4) for radiating soot particles [21].

$$\varepsilon_\lambda(KL, \lambda) = 1 - e^{-\frac{KL}{\lambda^a}} \quad (4)$$

where $\varepsilon_\lambda(KL, \lambda)$ is the spectral emissivity, K is the absorption coefficient, L is the thickness of the flame along the line-of-sight (m), and KL , which can be treated as a whole called the optical thickness [27], is an empirical parameter that depends on the wavelength in the visible range and can be considered a fixed value of 1.39 [24]. Substituting Equation (4) and (2) into Equation (3), we can obtain the following relationship between radiation intensity, KL , and T .

$$I_\lambda(T, \lambda) = \frac{1}{\pi} (1 - e^{-\frac{KL}{\lambda^a}}) \frac{C_1}{\lambda^5} \frac{1}{\exp \frac{C_2}{\lambda T} - 1} \quad (5)$$

KL and T are the only unknown parameters in the expression. However, for a spectrometer, the output consists of a radiation signal at multiple wavelengths. Thus, there are additional equations for the radiation intensity, KL , and T , so that the number of equations is greater than the number of unknown parameters. To solve the equations, a nonlinear least squares method is applied for

calculating KL and T . The value of KL , which is independent of the wavelength, can then be used in Equation (4) to determine the spectrally dependent ε_λ .

The measurement principle of temperature and emissivity described above is applied to the continuous spectrum. For the flame emission spectrum, which contains both discontinuous and continuous spectra, it is inappropriate to apply the above measurement principle. Indeed, flame emission spectra can be expressed as the sum of the continuous and discontinuous spectral emissions, as shown in Equation (6) [15].

$$E_e = E_c + E_d \quad (6)$$

The objective is to obtain the continuous flame emission E_c from the measured E_e using a simple method based on polynomial fitting. Subsequently, the discontinuous spectral emissions E_d can be estimated. The procedure of the method is summarized below:

- (i). The narrow bands corresponding to the discontinuous emissions, such as Na^* and K^* , are removed from the emitted flame spectrum E_e . The rest of the flame emission spectra can be expressed with E_{re} .
- (ii). A fifth-order polynomial fitting is used for E_{re} . The correlation coefficient R is used to evaluate the fitting results. If R is greater than 0.9999, it indicates that the fitting result is satisfactory. Subsequently, the fitting expression can be obtained for the estimated continuous flame emission.
- (iii). The wavelengths of the entire spectrum, selected for the calculation of temperature and emissivity, are incorporated into the obtained fitting expression. This allows us to estimate the continuous flame emission over a wide wavelength region.

The Hottel and Broughton emissivity model was used to test the accuracy of the method. Three groups of hypothesis values of KL and T were used to obtain a simulated continuous spectral baseline by integrating Planck's Law, as shown in Figure 1. Three simulated discontinuous emission bands were assumed based on a Gaussian function, as shown in Figure 2. Three types of white noise determined by the WGN (white Gaussian noise) function in Matlab (R2012a, The MathWorks, Inc., Natick, MA, USA) were used as simulated spectrometer noise, as shown in Figure 3. The power of the output noise at 80, 120, and 150 dBW was denoted by the capital letter P . Nine synthetic spectra were obtained by the combination of different simulated baselines, and the simulated discontinuous bands and the types of simulated noise were considered as the measured flame spectra, as shown in Figure 4. The wavelength interval of the simulated baseline, the discontinuous bands, and the noise between two adjacent wavelengths was set to 0.5 nm to facilitate a spectral synthesis.

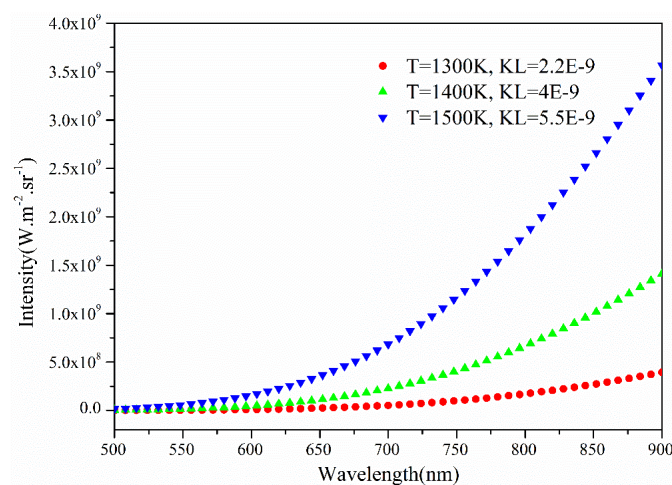


Figure 1. Simulated continuous spectral baseline.

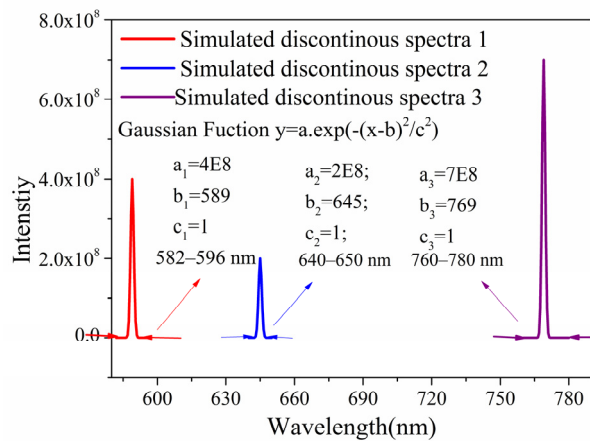


Figure 2. Simulated discontinuous spectral bands.

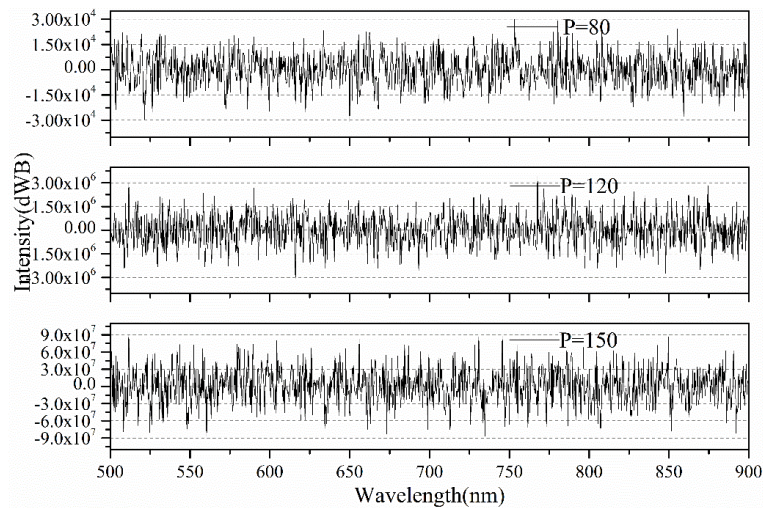


Figure 3. Three types of simulated noise spectra with different p values.

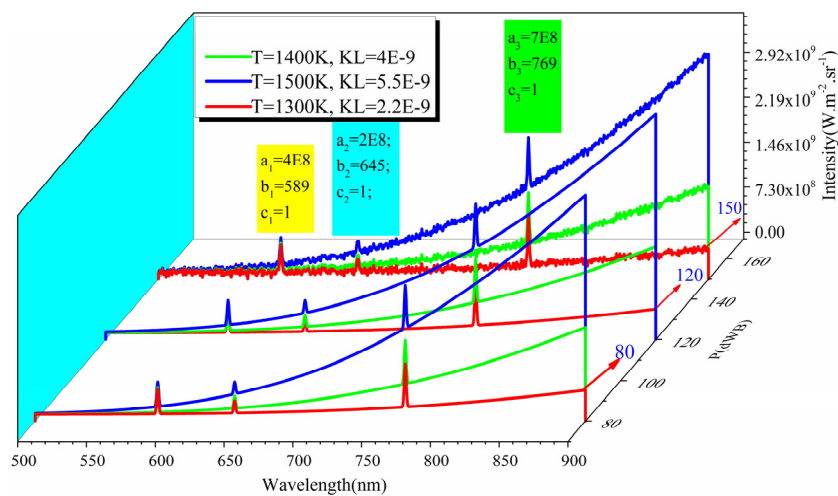


Figure 4. Nine simulated flame radiation spectra for different types of white noise.

There are nine synthetic spectra with different baselines and different types of white noise. The proposed method for separating the continuous baseline from the measured spectra was used to obtain

the estimated continuous spectrum. A nonlinear least squares method was applied to calculate the inverse temperature KL_1 and T_1 . The comparison between the predicted values of KL , T , and the inverse calculated KL_1 and T_1 values are shown in Table 1. The relative error of the predicted and inverse calculated values is also presented. The synthetic spectra with low white noise generally have a high accuracy. As the white noise increased, the accuracy of this method decreased. Furthermore, the stronger the intensity of the hypothesis baseline, the higher the precision for the inverse calculated KL_1 and T_1 is. This implies that the signal-to-noise ratio (SNR) will affect the accuracy of the method. For this example, the effect of the SNR is greater for KL than for T . However, for most synthetic spectra, the influence on the calculated KL and T values is acceptable. We conclude that the proposed method for separating the continuous and discontinuous spectra under a high SNR is appropriate.

Table 1. Predicted and calculated values with different types of white noise.

P	T	KL	T_1	KL_1	$ffiT$	$ffiKL$
80	1300	2.2×10^{-9}	2.20×10^{-9}	1299.988	0	0
	1400	4×10^{-9}	4.00×10^{-9}	1399.978	0	0
	1500	5.5×10^{-9}	5.50×10^{-9}	1499.976	0	0
120	1300	2.2×10^{-9}	2.17×10^{-9}	1300.873	0.06%	1.3%
	1400	4×10^{-9}	3.99×10^{-9}	1400.177	0	0.25%
	1500	5.5×10^{-9}	5.50×10^{-9}	1500.043	0	0
150	1300	2.2×10^{-9}	1.91×10^{-9}	1310.512	0.77%	13%
	1400	4×10^{-9}	3.85×10^{-9}	1402.391	0.17%	3.75%
	1500	5.5×10^{-9}	5.47×10^{-9}	1500.272	0	0.54%

3. Spectroscopic System and Calibration Introduction

The spectrometer system includes a laptop, universal serial bus (USB) data cable, portable spectrometer, optical fiber, fiber optic probe, and triangle bracket used for fixing the fiber optic probe (Figure 5). An AvaSpec-ULS2048-USB2 with a 2048 pixel CCD (Charge-coupled Device) detector array is used to process the incoming light data. A choice of 15 different gratings with different dispersions and blaze angles enables applications in the 200–1100 nm range. The fiber-optic spectrometer's integration time ranges from 1.1 to 600 ms, and the resolution of the spectrometer is 0.1 nm. During the measurement, the flame radiation is projected to an optical fiber after lens convergence and the signal is transmitted to the CCD fiber-optic spectrometer by optical fiber; subsequently, the obtained flame radiation spectrum signal is input into a computer for processing.

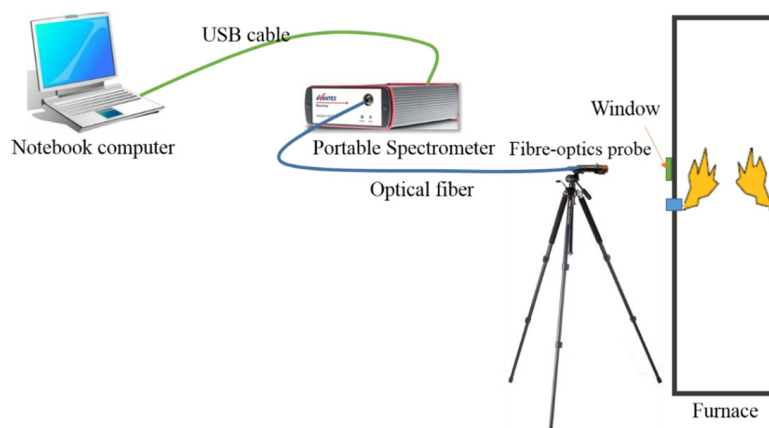


Figure 5. Schematic diagram of the spectrometer-based flame temperature measurement system. USB: universal serial bus.

A spectrometer system is used to obtain the monochromatic radiation intensity within a certain wavelength range. However, the signal output from the spectrometer is a voltage signal converted by photoelectric conversion [13]. To obtain the monochromatic radiation intensity, a calibration is required for spectrometer output values. A blackbody furnace with a temperature range from 300 °C to 1700 °C, model Mikron M330, is used for the calibration. The calibration factor as a function of λ yields the performance calibration curve with a wavelength ranging from 500 to 1100 nm at five temperatures of 1100 °C, 1200 °C, 1300 °C, 1400 °C, and 1500 °C.

In order to verify the accuracy of the calibration, the results before and after correction for 1100 °C and 1400 °C are shown in Figure 6, which shows that the measured spectral curves and the corrected curves are consistent with the theoretical results. The theoretical blackbody radiation intensity after calibration is essentially coincident with the blackbody radiation intensity at temperatures of 1200 °C, 1300 °C, 1400 °C, and 1500 °C, indicating that the calibration is accurate.

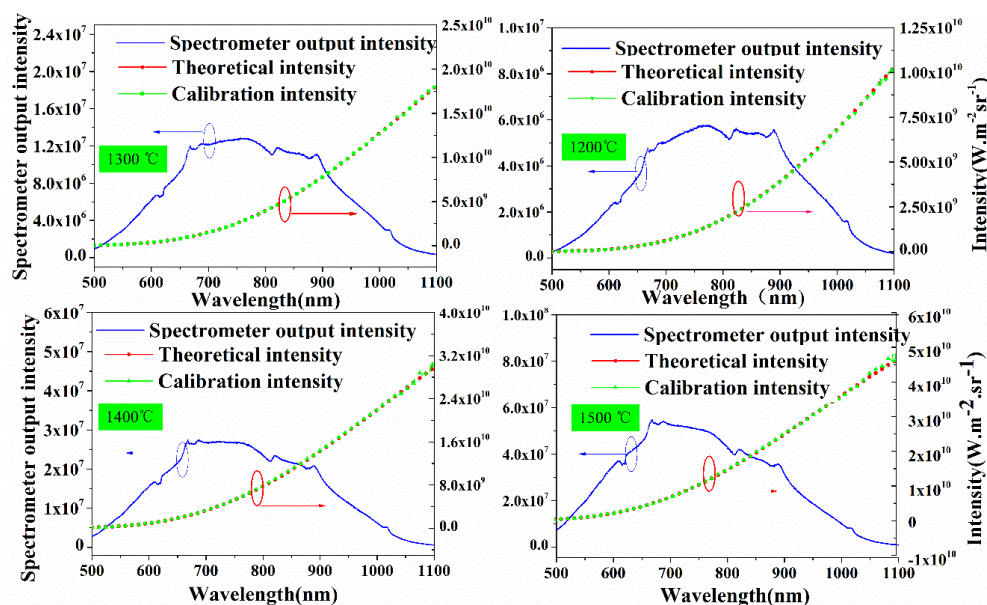


Figure 6. Spectra before and after calculation at 1200 °C, 1300 °C, 1400 °C, and 1500 °C.

4. Experimental Setup and Procedure

The measurements were conducted in a 1000 MW supercritical coal-fired boiler at the Huadian International Zouxian Power Plant. The boiler furnace has four layers of swirl burners and uses the opposed wall firing method, as shown schematically in Figure 7. In each layer, eight burners are equally distributed on the front and back furnace walls. The measurement points positioned in the 5.5 layer of the left wall were numbered #1 and #2; the measurement points in the 6 layer of the left wall were numbered #3, #4, #5, and #6; and the measurement points located in the 8.5 layer of the front wall were numbered #7, #8, #9, #10, #11, #12, #13, #14, #15, and #16. Finally, the measurement points in the center hole of the left and right wall in the 9 layer were numbered #17 and #18. The layers of the burners numbered from bottom to top were called the first, second, third, and fourth layer. The distance between the 9 layer and the fourth layer of the burners is 18.9 m, and there is a distance of 13.3 m from the 8.5 layer to the fourth layer of the burners. The 6 layer is 2.5 m from the fourth layer of the burners. All of the described layers are at the top of the fourth layer of the burners; however, the 5.5 layer is located between the third layer of the burners and the fourth layer of the burners. The measurement points of the 5.5 layer are close to the third distribution layer of the burners and the distance is 3.3 m.

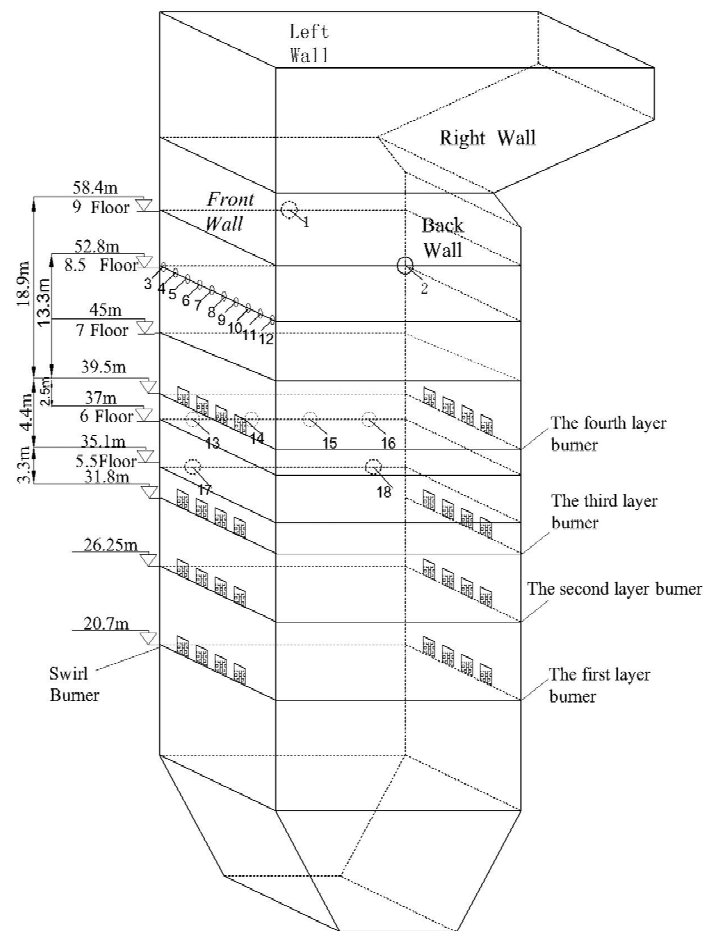


Figure 7. Schematic diagram of the furnace and locations of measuring points in the 1000 MW unit.

During the measurements, the boiler load of the unit remained unchanged and the 1000 MW unit operated at 992 MW. The spectrometer measurements were performed at different locations in the unit. The raw output data from the spectrometer system was calibrated and used for the spectral analysis and calculation of the flame's temperature and emissivity. During spectrum acquisition, the optical fiber probe was placed perpendicular to the wall of the observation points. The measurement points in the unit were named from bottom to top to facilitate the analysis and discussion. To reduce the measurement error caused by the disturbance of the pulverized coal flame when measuring each point, multiple groups of spectral data were collected at each measurement point and the average value of the flame radiation intensity for the points under the same boiler load was calculated.

5. Experimental Results and Analysis

5.1. Spectral Analysis of Coal-Fired Flame and Baseline Removal

The calibrated intensity profiles at 8 of the 18 measurement points in the boiler are shown in Figure 8. Na^* and Li^* radiate at 589 nm and 670.4 nm, respectively, and exist in several calibrated intensity profiles. The intensity of Na^* and Li^* is very weak, and even difficult to detect in some profiles. K^* , located at 766.5 nm and 769.9 nm, was observed in most profiles. Rb^* , located at 779.4 nm and 793.8 nm, was also found in several profiles. Interestingly, the alkali metal radiation was not very strong even though it commonly exhibits strong spectral radiation. The strongest alkali metal radiation occurred at position #11, but the spectral intensity at this position was not the highest. The proposed baseline separation method was used to estimate the continuous spectra. Additionally, the

goodness-of-fit coefficient (GFC) metric was applied to evaluate the reliability of the proposed method for baseline removal. The GFC metric is based on Schwartz's inequality and is defined as [13]:

$$GFC = \frac{\left| \sum_j E_e(\lambda_j) \hat{E}_c(\lambda_j) \right|}{\left[\sum_j [E_e(\lambda_j)]^2 \right]^{\frac{1}{2}} \left[\sum_j [\hat{E}_c(\lambda_j)]^2 \right]^{\frac{1}{2}}} \quad (7)$$

Generally, an accurate estimation yields a GFC of [0.995, 0.999], and a GFC of [0.999, 0.9999] indicates a good spectral match while a GFC larger or equal to 0.9999 is an excellent spectral match [13]. The GFC values of the selected profiles are shown in Table 2. The GFC values are very high for eight measurement points, and the estimated continuous spectra indicate an excellent spectral match. This again proves the feasibility of the proposed method. The baseline removal results for six observation points are presented in Figure 9. Six recovered discontinuous spectra of the measured flame emission spectrum are shown in Figure 10.

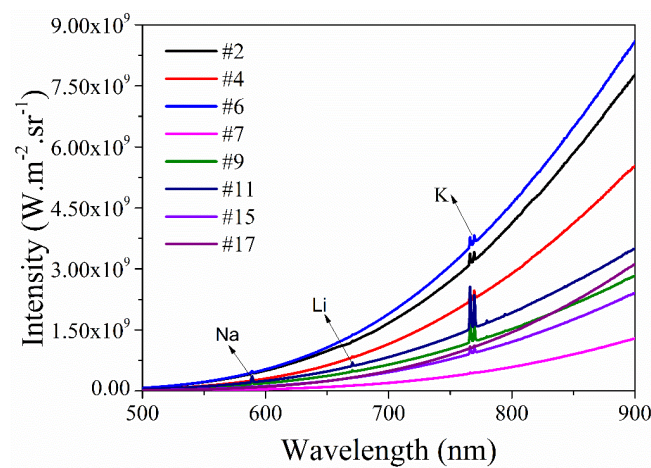


Figure 8. Calibrated intensity profiles of coal flames measured at eight of the eighteen measurement points.

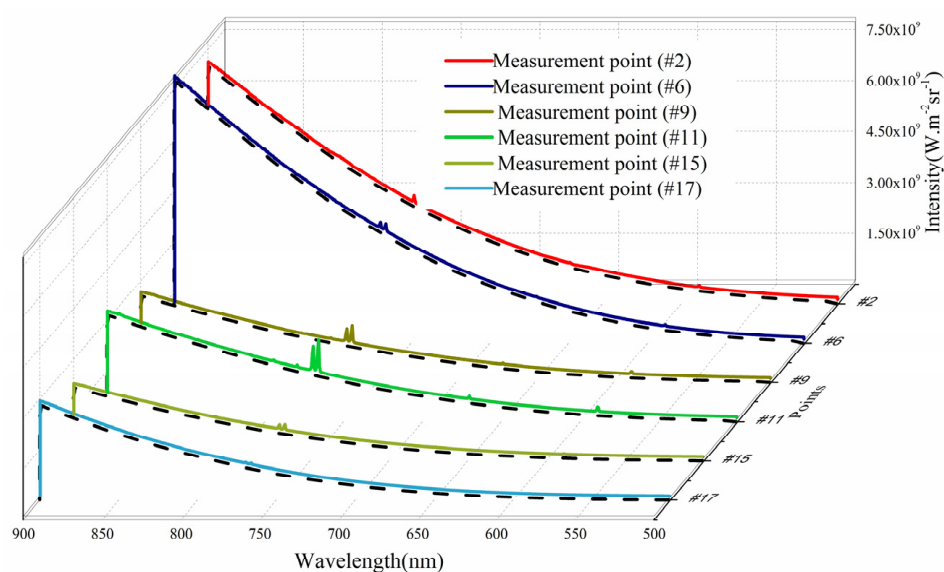


Figure 9. Baseline removal results for six observation points.

Table 2. The goodness-of-fit coefficient (GFC) values of selected profiles.

Points	#2	#4	#6	#7	#9	#11	#15	#17
GFC	0.9999	0.9999	0.9999	0.9992	0.9996	0.9992	0.9999	0.9994

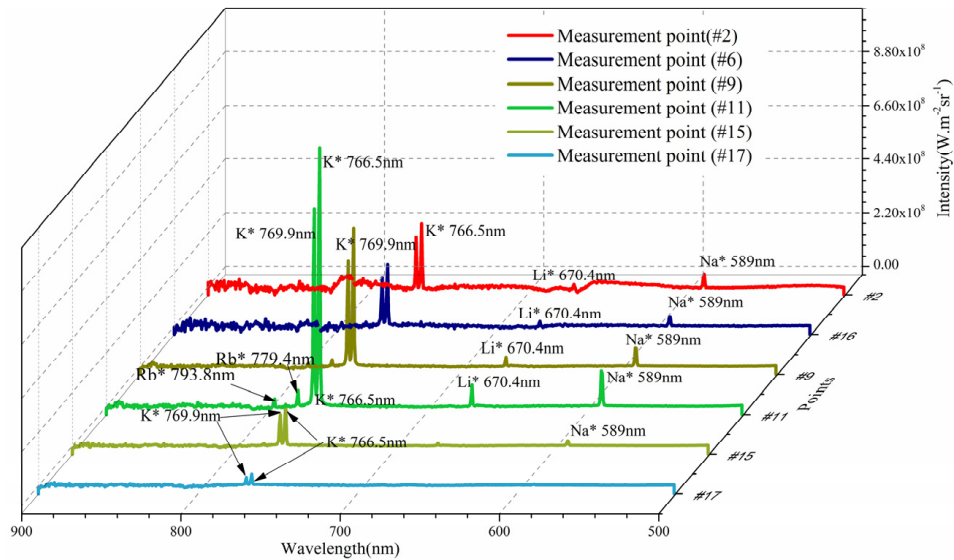


Figure 10. Discontinuous spectra separated from the flame radiation spectrum.

5.2. The Effect of Separated Discontinuous Spectra on Temperature and Emissivity Measurements

The influence of the separated discontinuous spectra on the calculation of temperature and emissivity was evaluated by comparing the calculated temperature and emissivity values before and after the separation of the discontinuous spectra. The Hottel and Broughton emissivity model was used for the calculations, and the differences in the calculated temperature and emissivity values were analyzed in detail as shown in Figures 11 and 12. It is worth noting that the calculated temperature and radiation intensity values of the alkali metal are referred to as the apparent value.

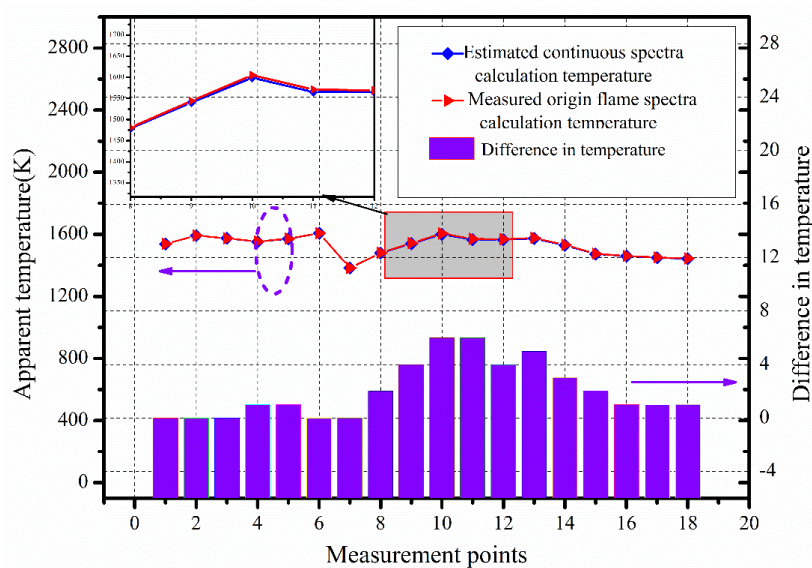


Figure 11. Influence of radiation intensity of discontinuous emission spectra on the temperature calculation.

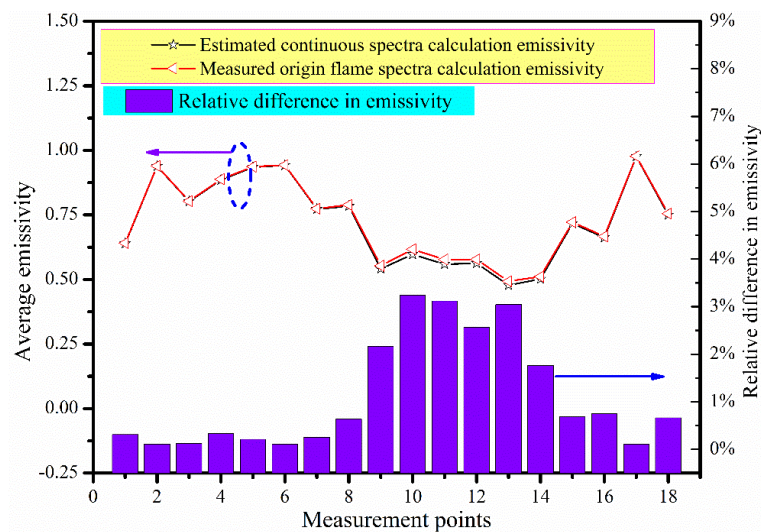


Figure 12. Influence of radiation intensity of discontinuous emission spectra on the calculation of average emissivity.

There was only a small difference in the calculated temperature and emissivity values based on the estimated continuous spectra and the emitted flame spectrum. The maximum difference in the apparent temperature appeared in #10 and was only 6 K. The impact on the differences in emissivity was relatively small and similar to the observed influence on the calculation of the apparent temperature. The maximum relative difference for all points was less than 5%, as shown in Figure 12. This finding indicated that the spectra separation was not required for the calculation of apparent temperature and emissivity. However, the separation was performed to analyze the relationship between the apparent radiation intensity of the alkali metal and the apparent temperature based on the Hottel and Broughton model.

In coal, alkali metals are primarily present as simple salts, indicating that they can easily enter the gas phase during combustion. The presence of alkali salts in deposits may cause accelerated corrosion at temperatures well below the melting point [28]. At the same time, the corrosion caused by chlorine is closely linked to the presence of alkali metals in the deposits. For this reason, accurate measurements of alkali metals, such as Na^* and K^* , in a flame are important for the prevention of coking in a furnace. In fact, the concentration of the gas phase alkali metal relates to both the radiation intensity of the alkali metal and also the local temperature. However, there has been limited research on the relationship between these three factors. In this study, the alkali metals K^* and Na^* were used as an example to analyze the relationship between temperature and radiation intensity at the same measuring position.

The actual radiation intensity of the alkali metals Na^* and K^* can be determined by the proposed spectral separation method. The relationship between the radiation intensity of alkali metals and temperature has been investigated in other studies. Yan et al. [21] demonstrated that alkali emissions increased with increasing temperature. The relationship between temperature and radiation intensity of the alkali metals at different measured points is shown in Figure 13. The apparent radiation intensity of K^* and Na^* exhibits a very consistent trend and roughly the same change trend as the calculated apparent temperature, as described previously [21]. However, there is no specific function between these factors, but this occurs because the radiation intensity of the alkali metal is related to the measurement location of the flame's temperature and the gas phase alkali metal concentrations. In locations far from the burner, the radiation intensity of the alkali metal is weak. This is mainly attributed to the fact that the spectral radiation intensity of the alkali metal and the excitation temperature are closely related; at temperatures lower than the alkali excitation temperature, the alkali metal is unable to affect the spectral intensity.

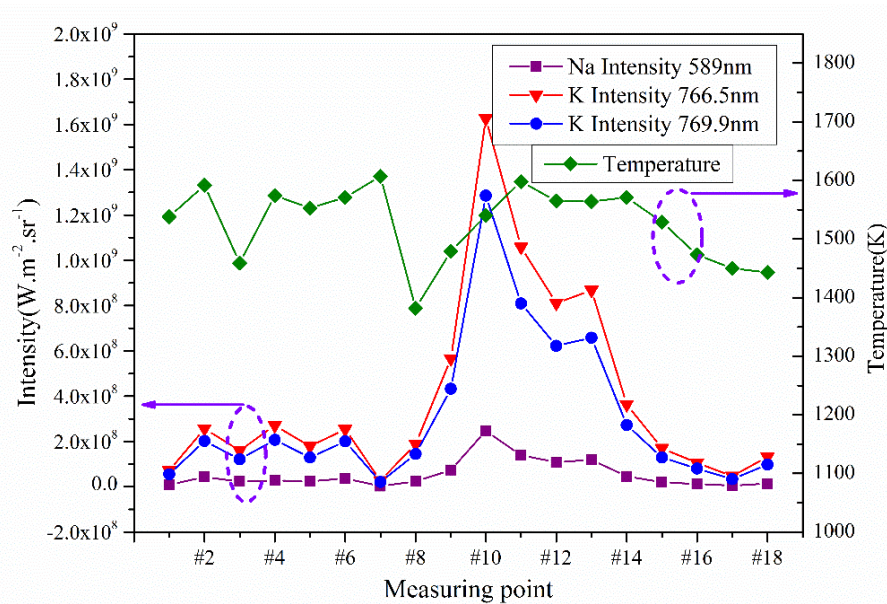


Figure 13. Relationship between actual radiation of alkali metal and calculated temperature at different measurement points.

6. Conclusions

A fiber-optic spectrometer was used for the diagnosis of a 1000 MW coal-fired power plant boiler furnace. The calibration of the spectrometer was conducted in a blackbody furnace to obtain the calibration coefficient, and the accuracy of the calibration coefficient was confirmed.

A simple method was proposed to separate the baseline from the continuous and discontinuous spectra. The accuracy of the estimated continuous baseline derived from the measured flame spectra was evaluated by the goodness-of-fit coefficient and satisfactory agreements were achieved for the selected profiles. The influence of the discontinuous emission spectra on the calculations of temperature and emissivity for several observation points was evaluated for a coal-fired flame. There was little difference in the calculated temperature and emissivity based on the estimated continuous spectra and the emitted flame spectrum, and the maximum difference for the temperature for all measurement points was only 6 K. The impact on emissivity was very small and similar to the influence on the calculated temperature, and the relative difference in emissivity at all points was less than 5%.

A comparison between the actual intensity of the alkali metal and the calculated temperature indicated that the change in the radiation intensity of the alkali metal followed the trend of the calculated temperature. However, this was not consistent with the relationship between the radiation intensity of the alkali metal and the calculated temperature. This implies that the radiation intensity of the alkali metal is related to the measurement location of the flame's temperature and the alkali metal concentrations.

Acknowledgments: The present study has been supported by the Natural Science Foundation of Jiangsu Province (No. BK20150174, No. BK20140187). This work is also supported by Natural Science Foundation of China (No. 51706239, No. 51706240).

Author Contributions: Weijie Yan conceived and designed the experiments; Weijie Yan, Yunqi Ya, and Feng Du performed the experiments; Weijie Yan, Hao Shao, and Peitao Zhao analyzed the data; and Weijie Yan wrote the paper.

Conflicts of Interest: The founding sponsors had no role in the design of the study; in the collection, analyses, or interpretation of data; in the writing of the manuscript, and in the decision to publish the results.

References

1. Giraud, J.H.; Gee, K.L.; Ellsworth, J.E. Acoustic temperature measurement in a rocket noise field. *J. Acoust. Soc. Am.* **2010**, *127*, E1179–E1184. [[CrossRef](#)] [[PubMed](#)]
2. Yan, W.J.; Zheng, S.; Zhou, H.C. Experiments investigation on 2D distribution of soot temperature and volume fraction by image processing of visible radiation. *Appl. Therm. Eng.* **2017**, *124*, 1014–1022. [[CrossRef](#)]
3. Lee, W.D.; Han, K.; Hahn, J.W. Direct determination of effective spectral emissivity of hot burnt gas using absolutely calibrated radiometric spectrometer. *Propellants Explos. Pyrotech.* **2017**, *42*, 558–565. [[CrossRef](#)]
4. Yan, W.J.; Chen, D.M.; Yang, Z.M.; Yan, E.Y.; Zhao, P.T. Measurement of Soot Volume Fraction and Temperature for Oxygen-Enriched Ethylene Combustion Based on Flame Image Processing. *Energies* **2017**, *10*, 750. [[CrossRef](#)]
5. Yan, W.J.; Lou, C. Two-dimensional distributions of temperature and soot volume fraction inverted from visible flame images. *Exp. Therm. Fluid Sci.* **2013**, *50*, 229–233. [[CrossRef](#)]
6. Weinrotter, M.; Kopecek, H.; Tesch, M.; Wintner, E.; Lackner, M.; Winter, F. Laser ignition of ultra-lean methane/hydrogen/air mixtures at high temperature and pressure. *Exp. Therm. Fluid Sci.* **2005**, *29*, 569–577. [[CrossRef](#)]
7. Brisley, P.M.; Lu, G.; Yan, Y.; Cornwell, S. Three-dimensional temperature measurement of combustion flames using a single monochromatic CCD camera. *IEEE Trans. Instrum. Meas.* **2005**, *54*, 1417–1421. [[CrossRef](#)]
8. Zabrodiec, D.; Hees, J.; Massmeyer, A.; vom Lehn, F.; Habermehl, M.; Hatzfeld, O.; Kneer, R. Experimental investigation of pulverized coal flames in CO₂/O₂– and N₂/O₂-atmospheres: Comparison of solid particle radiative characteristics. *Fuel* **2017**, *201*, 136–147. [[CrossRef](#)]
9. Liu, D.; Yan, J.H.; Wang, F.; Huang, Q.X.; Chi, Y.; Cen, K.F. Experimental reconstructions of flame temperature distributions in laboratory-scale and large-scale pulverized-coal fired furnaces by inverse radiation analysis. *Fuel* **2012**, *93*, 397–403. [[CrossRef](#)]
10. Yan, W.J.; Zhou, H.C.; Jiang, Z.W.; Lou, C.; Zhang, X.K.; Chen, D.L. Experiments on measurement of temperature and emissivity of municipal solid waste (msw) combustion by spectral analysis and image processing in visible spectrum. *Energy Fuel* **2013**, *27*, 6754–6762. [[CrossRef](#)]
11. Sun, Y.P.; Lou, C.; Zhou, H.C. A simple judgment method of gray property of flames based on spectral analysis and the two-color method for measurements of temperatures and emissivity. *Proc. Combust. Inst.* **2011**, *33*, 735–741. [[CrossRef](#)]
12. Monkhouse, P. On-line spectroscopic and spectrometric methods for the determination of metal species in industrial processes. *Prog. Energy Combust. Sci.* **2011**, *37*, 125–171. [[CrossRef](#)]
13. Parameswaran, T.; Hughes, R.; Gogolek, P.; Hughes, P. Gasification temperature measurement with flame emission spectroscopy. *Fuel* **2014**, *134*, 579–587. [[CrossRef](#)]
14. Schulze, G.; Jirasek, A.; Yu, M.M.L.; Lim, A.; Turner, R.F.B.; Blades, M.W. Investigation of selected baseline removal techniques as candidates for automated implementation. *Appl. Spectrosc.* **2005**, *59*, 545–574. [[CrossRef](#)] [[PubMed](#)]
15. Arias, L.; Sbarbaro, D.; Torres, S. Removing baseline flame's spectrum by using advanced recovering spectrum techniques. *Appl. Opt.* **2012**, *51*, 6111–6116. [[CrossRef](#)] [[PubMed](#)]
16. Oleschko, H.; Schimroszyk, A.; Lippert, H.; Muller, M. Influence of coal composition on the release of Na-, K-, Cl-, and S-species during the combustion of brown coal. *Fuel* **2007**, *86*, 2275–2282. [[CrossRef](#)]
17. Cai, X.S.; Cheng, Z.H.; Wang, S.M. Flame measurement and combustion diagnoses with spectrum analysis. In *Multiphase Flow: The Ultimate Measurement Challenge*; Cai, X., Wu, Y., Huang, Z., Wang, S., Wang, M., Eds.; American Institute of Physics: College Park, MD, USA, 2007; pp. 60–66.
18. Sabel, T.; Unterberger, S.; Hein, K. Application of quotient pyrometry to industrial pulverised coal combustion. *Exp. Therm. Fluid Sci.* **2002**, *26*, 283–289. [[CrossRef](#)]
19. Zhou, H.C.; Lou, C.; Cheng, Q.; Jiang, Z.W.; He, J.; Huang, B.Y.; Pei, Z.L.; Lu, C.X. Experimental investigations on visualization of three-dimensional temperature distributions in a large-scale pulverized-coal-fired boiler furnace. *Proc. Combust. Inst.* **2005**, *30*, 1699–1706. [[CrossRef](#)]
20. Wang, F.; Wang, X.J.; Ma, Z.Y.; Yan, J.H.; Chi, Y.; Wei, C.Y.; Ni, M.J.; Cen, K.F. The research on the estimation for the NO_x emissive concentration of the pulverized coal boiler by the flame image processing technique. *Fuel* **2002**, *81*, 2113–2120.

21. Yan, W.J.; Lou, C.; Cheng, Q.; Zhao, P.T.; Zhang, X.Y. In situ measurement of alkali metals in an msw incinerator using a spontaneous emission spectrum. *Appl. Sci.* **2017**, *7*, 263. [[CrossRef](#)]
22. Draper, T.S.; Zeltner, D.; Tree, D.R.; Xue, Y.; Tsiava, R. Two-dimensional flame temperature and emissivity measurements of pulverized oxy-coal flames. *Appl. Energy* **2012**, *95*, 38–44. [[CrossRef](#)]
23. Backstrom, D.; Gall, D.; Pushp, M.; Johansson, R.; Andersson, K.; Pettersson, J.B.C. Particle composition and size distribution in coal flames—The influence on radiative heat transfer. *Exp. Therm. Fluid Sci.* **2015**, *64*, 70–80. [[CrossRef](#)]
24. Fletcher, T.H.; Ma, J.L.; Rigby, J.R.; Brown, A.L.; Webb, B.W. Soot in coal combustion systems. *Prog. Energy Combust.* **1997**, *23*, 283–301. [[CrossRef](#)]
25. Choi, S.K.; Choi, B.C.; Lee, S.M.; Choi, J.H. The effect of liquid fuel doping on PAH and soot formation in counterflow ethylene diffusion flames. *Exp. Therm. Fluid Sci.* **2015**, *60*, 123–131. [[CrossRef](#)]
26. Modest, M.F. *Radiative Heat Transfer*, 2nd ed.; Academic Press: Cambridge, MA, USA, 2003.
27. Arias, L.; Torres, S.; Sbarbaro, D.; Ngendakumana, P. On the spectral bands measurements for combustion monitoring. *Combust. Flame* **2011**, *158*, 423–433. [[CrossRef](#)]
28. Nielsen, H.P.; Frandsen, F.J.; Dam-Johansen, K.; Baxter, L.L. The implications of chlorine-associated corrosion on the operation of biomass-fired boilers. *Prog. Energy Combust.* **2000**, *26*, 283–298. [[CrossRef](#)]



© 2017 by the authors. Licensee MDPI, Basel, Switzerland. This article is an open access article distributed under the terms and conditions of the Creative Commons Attribution (CC BY) license (<http://creativecommons.org/licenses/by/4.0/>).